Enhanced Bonding of Gold Nanoparticles on Oxidized TiO2(110)

ARTICLE *in* SCIENCE · APRIL 2007

Impact Factor: 33.61 · DOI: 10.1126/science.1135752 · Source: PubMed

8 AUTHORS, INCLUDING:

Stefan Wendt
Aarhus University
54 PUBLICATIONS **2,826** CITATIONS
SEE PROFILE

Renald Schaub
University of St Andrews
27 PUBLICATIONS **2,316** CITATIONS
SEE PROFILE

Erik Lægsgaard
Aarhus University
276 PUBLICATIONS **14,654** CITATIONS
SEE PROFILE

Flemming Besenbacher
Aarhus University
643 PUBLICATIONS **25,682** CITATIONS
SEE PROFILE

Enhanced Bonding of Gold Nanoparticles on Oxidized TiO_2(110)

D. Matthey, J. G. Wang, S. Wendt, J. Matthiesen, R. Schaub, E. Lægsgaard, B. Hammer, F. Besenbacher*

We studied the nucleation of gold clusters on TiO_2(110) surfaces in three different oxidation states by high-resolution scanning tunneling microscopy. The three TiO_2(110) supports chosen were (i) reduced (having bridging oxygen vacancies), (ii) hydrated (having bridging hydroxyl groups), and (iii) oxidized (having oxygen adatoms). At room temperature, gold nanoclusters nucleate homogeneously on the terraces of the reduced and oxidized supports, whereas on the hydrated TiO_2(110) surface, clusters form preferentially at the step edges. From interplay with density functional theory calculations, we identified two different gold-TiO_2(110) adhesion mechanisms for the reduced and oxidized supports. The adhesion of gold clusters is strongest on the oxidized support, and the implications of this finding for catalytic applications are discussed.

The discovery of distinctive catalytic properties of dispersed gold nanoparticles on oxide supports (*1*, *2*) has stimulated extensive research activities (*2*–*5*), and a general consensus now exists on several aspects of this system. The size of the gold particles substantially affects the catalytic activity, and the gold clusters must be smaller than 5 nm for high catalytic activity to occur (*6*–*8*). The choice of the oxide support influences the catalytic activity, so there is a strong "support effect" in addition to the "size effect" (*2*, *4*, *9*), and reducible oxides are advantageous as compared to nonreducible ones (*9*, *10*). However, the relation of the adhesion properties of nanosized gold with catalytic activity is still unresolved. A number of studies (mainly catalysis work done on high area support materials) have reported that slightly oxidized gold ($Au^{+\delta}$), in addition to metallic gold (Au^0), is important to achieve high activity of dispersed Au catalysts (*2*, *4*, *11*–*16*). In parallel, several surface science studies of model systems favored an interpretation where oxygen vacancies have been invoked as being responsible for the stabilization and activity of Au clusters on the support (*17*–*20*).

We studied the fundamental mechanisms of metal oxide–support adhesion by means of scanning tunneling microscopy (STM) and density functional theory (DFT) calculations. We compare the nucleation of Au clusters on one support material that had been prepared in different oxidation states. We chose rutile TiO_2(110) as the model support because numerous studies exist on the Au/TiO_2 model system, and Au/TiO_2 is a good catalyst for CO oxidation at low temperatures, as shown in the pioneering studies by Haruta (*1*, *6*), Goodman (*7*, *18*), and the work of others (*21*–*23*).

Interdisciplinary Nanoscience Center (iNANO) and Department of Physics and Astronomy, University of Aarhus, DK-8000 Aarhus C, Denmark.

*To whom correspondence should be addressed. E-mail: fbe@inano.dk

The TiO_2(110) surface consists of alternating rows of fivefold-coordinated Ti (5f-Ti) atoms and protruding, twofold-coordinated bridging oxygen (O_{br}) atoms. The Ti atoms underneath the O_{br} atoms are sixfold coordinated as any other Ti atom in stoichiometric rutile. An Ar^+ sputtered and vacuum-annealed TiO_2(110) crystal is an n-type semiconductor, and its surface has a number of O_{br} vacancies (*5*). The STM images of the TiO_2(110) surface are dominated by electronic effects (i.e., bright rows correspond to the Ti troughs), whereas geometrically protruding O_{br} atoms appear dark (*5*). Accordingly, the faint spots that connect the bright Ti troughs arise from O_{br} vacancies (Fig. 1A) (*24*).

Starting with a clean, reduced TiO_2(110) [*r*-TiO_2(110)] surface, we prepared two further well-defined TiO_2(110) surfaces under ultrahigh vacuum conditions (*24*, *25*). First, we produced a hydrated TiO_2(110) [*h*-TiO_2(110)] surface with H adatoms, capping some of the O_{br} atoms by letting water dissociate in O_{br} vacancies (Fig. 1B). The capping H atoms form bridging hydroxyls (OH_{br}) that appear as brighter protru-

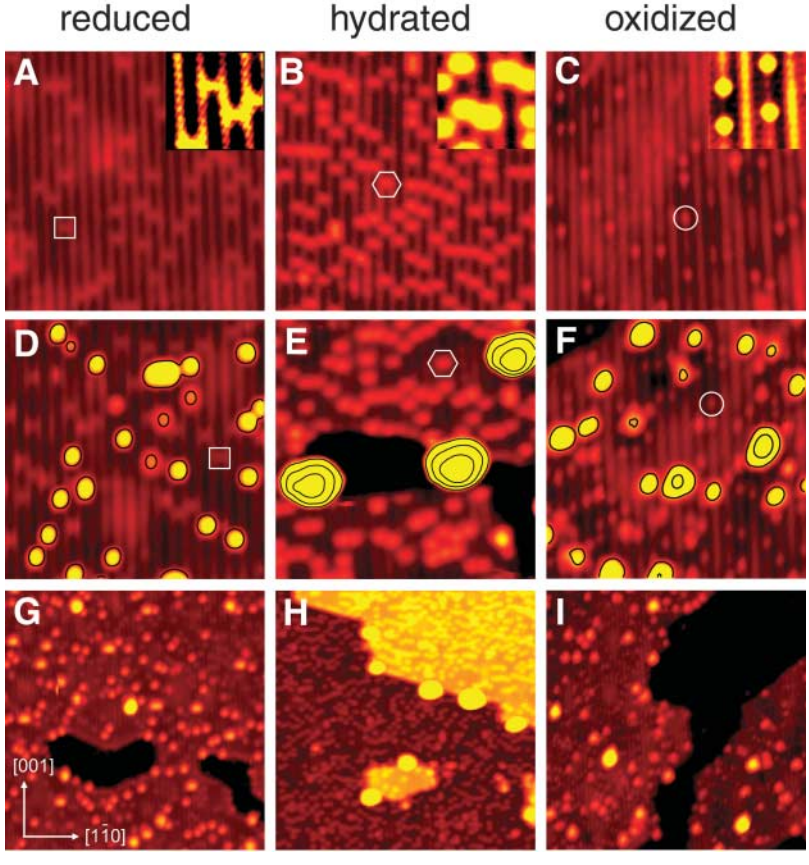

Fig. 1. STM images of *r*- (**A**), *h*- (**B**), and *o*- (**C**) TiO_2(110) surfaces before Au exposure (130 × 130 Å^2). Symbols indicate O_{br} vacancies (square), H adatoms on O_{br} sites (hexagon), and O_{ot} atoms in the Ti troughs (circle). Insets (30 × 30 Å^2) show the point defects of interest enlarged. For the detailed preparation recipes, see (*25*). (**D** to **I**) STM images after 3% ML Au exposure at RT [1 ML is defined as 1.387×10^{15} atoms per cm^2 corresponding to Au(111)]. Image sizes are 130 × 130 Å^2 [(D) to (F)] and 350 × 350 Å^2 [(G) to (I)], respectively. In [(D) to (F)], the heights of the Au clusters are given by contour lines at 1.2, 3.2, and 5.2 Å above the terrace. Directions are as indicated in (G), and tunnel parameters (tunneling current $I_t \leq 0.1$ nA, tunneling voltage $V_t = 1.2$ V) are identical throughout the paper.

sions between the Ti rows than those associated with the O_{br} vacancies (*24*, *26*). Second, we prepared an oxidized TiO_2(110) [*o*-TiO_2(110)] surface by letting O_2 dissociate in O_{br} vacancies (*24*, *27*), resulting in an *o*-TiO_2(110) surface characterized by perfect O_{br} rows and by a number of O adatoms (O_{ot}) located in the Ti troughs (Fig. 1C). These O_{ot} atoms show up in the STM images as protrusions distributed along the Ti troughs and are located on top of 5f-Ti sites (*24*, *26*).

After exposing these three different TiO_2(110) surfaces to Au [3% of a monolayer (ML)] at room temperature (RT), we observed quite different Au cluster morphologies. In case of the *r*-TiO_2(110) surface, numerous rather small Au clusters are distributed homogeneously on the terraces (Fig. 1, D and G). In contrast, on the *h*-TiO_2(110) surface, we found fairly large Au clusters that preferentially decorate the step edges of the substrate, and no small Au clusters on the terraces are seen (Fig. 1, E and H). However, on the *o*-TiO_2(110) surface, we again found Au clusters to nucleate homogeneously on the terraces (Fig. 1, F and I).

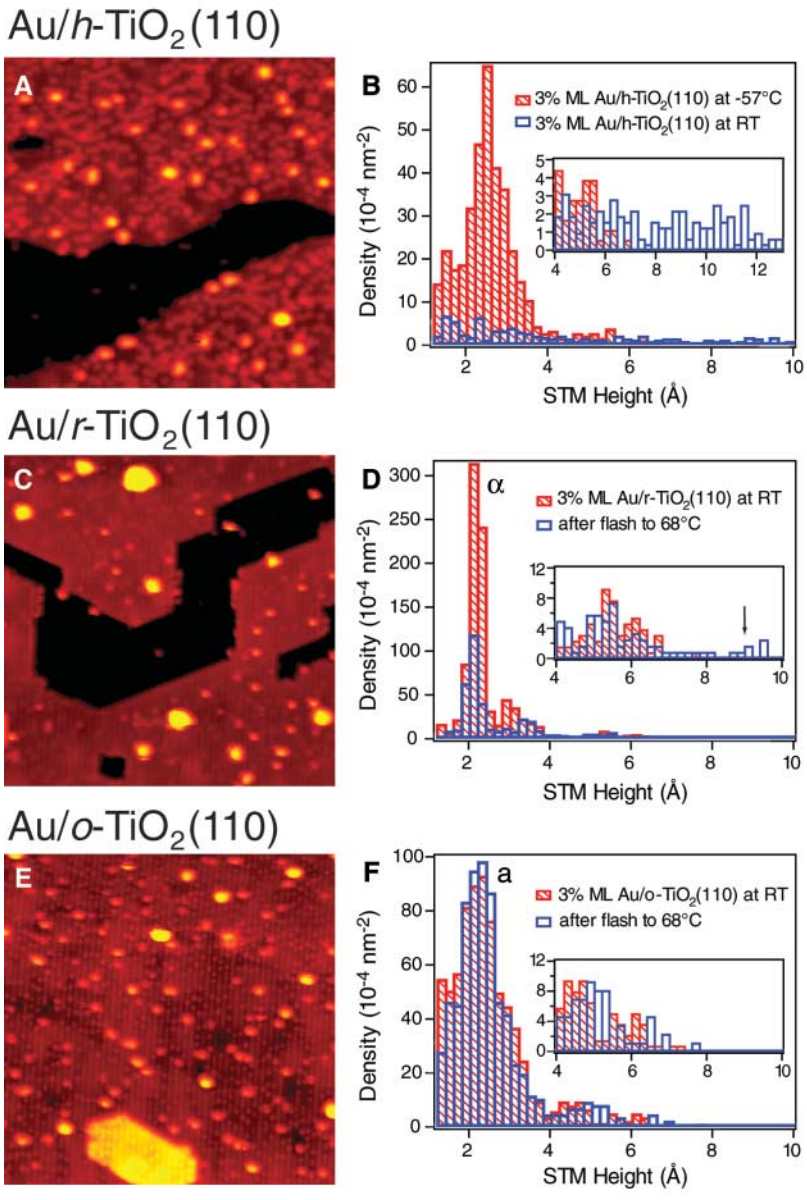

Fig. 2. (**A**) STM image of the *h*-TiO_2(110) surface after 3% ML Au exposure at –57°C (350 × 350 Å^2), and (**B**) Au height histograms corresponding to Au/*h*-TiO_2(110) surfaces for substrate temperatures of –57°C (hatched red bars) and RT (blue bars). The histograms rely on scanned areas of ~10^4 nm^2 each (~1000 Au clusters per histogram). A threshold of 1.2 Å above the terrace was chosen to ensure that exclusively Au clusters are considered for the histograms. (**C**) STM image of the Au/*r*-TiO_2(110) surface (350 × 350 Å^2) prepared by 3% ML Au deposition at RT followed by heating up to 68°C. (**D**) Au height histograms corresponding to Au/*r*-TiO_2(110) before (hatched red bars) and after (blue bars) heating of the sample. In (D), the peak indicated by "α" corresponds to Au_1 trapped in O_{br} vacancies. The arrow in the inset indicates large Au_n clusters that are a result of sintering. (**E** and **F**) Like (C) and (D) but for the Au/*o*-TiO_2(110) surface. In (F), the peak indicated by "a" corresponds to Au_n clusters of one layer height. No sintering was observed.

The absence of homogeneously distributed small Au nanoclusters on the *h*-TiO_2(110) surface implies that monomeric Au (Au_1) and small Au nanoclusters diffuse readily at RT on this surface. This finding is in agreement with previous RT-STM studies addressing Au/TiO_2(110) (*7*, *17*, *28*, *29*), where sintering of incoming Au_1 has been reported. In the present work, we found homogeneously distributed small Au clusters also on the terraces of the *h*-TiO_2(110) surface when we cooled the substrate down to –57°C before exposure (Fig. 2, A and B). According to these results, we infer that the interaction between Au clusters and the *h*-TiO_2(110) surface is fairly weak (*30*). On the contrary, both for the *r*-TiO_2(110) surface (with O_{br} vacancies) and the *o*-TiO_2(110) surface (with O_{ot} atoms), the results presented in Fig. 1 imply that, on these two TiO_2(110) surfaces, stronger Au-TiO_2 interactions occur than on the *h*-TiO_2(110) surface.

Given the stronger interactions with the *r*- and the *o*-TiO_2(110) surfaces, we explored the effect of heating on the Au cluster morphologies on these two TiO_2 surfaces (Fig. 2, C to F). Starting points in these experiments were *r*- and *o*-TiO_2(110) surfaces that we exposed to 3% ML Au at RT (Fig. 1, D and G and Fig. 1, F and I, respectively). After subsequent heating of the samples to 68°C, Au sintering is clearly evident for Au/*r*-TiO_2(110) (Fig. 2C) but not for Au/*o*-TiO_2(110) (Fig. 2E). The different stabilities of the Au clusters against sintering on the two TiO_2(110) surfaces considered are even more obvious when looking at the corresponding Au height histograms (Fig. 2, D and F). For reference, we also show the height histograms obtained on the Au exposed surfaces before heating (hatched red bars). After the heating of the Au/*r*-TiO_2(110) surface (blue bars in Fig. 2D), the sharp feature at Au cluster heights of 1.8 to 2.6 Å (labeled "α") is almost three times less intense than before. Because the "α" peak corresponds to Au_1 trapped in O_{br} vacancies (see below), this result indicates that about two-thirds of the Au_1 clusters have coalesced with other Au_n clusters. The sintering of Au_1/Au_n clusters on the *r*-TiO_2(110) surface leads to the formation of large Au_n clusters with STM heights up to 10 Å (Fig. 2D, inset). Nothing in the STM data points to the occurrence of a ripening mechanism. Instead, our data are consistent with coalescence of Au_n clusters as the prevailing sintering mechanism.

On the *o*-TiO_2(110) surface, the Au height histograms (Fig. 2F) show pronounced peaks of identical intensities at STM heights between 1.2 and 3.4 Å (labeled "a") both before and after heating of the sample. The characteristic "a" peak found for the Au/*o*-TiO_2(110) surface is less intense but broader than the narrow α peak typical for Au_1 on the *r*-TiO_2(110) surface. This result can be explained by the

existence of many stable Au_n cluster configurations on the *o*-TiO_2(110) surface, whereas only few stable Au_n cluster configurations seem to exist on the *r*-TiO_2(110) surface. The clear dependence of the Au height distribution on *r*-TiO_2(110) as opposed to the invariance of the distribution on *o*-TiO_2(110) upon heating to 68°C reveals that the Au_n clusters bind more strongly to the O-rich oxide support.

To rationalize the obtained Au cluster distributions after Au exposure at RT, we compared the diffusion of Au_1 on the three different TiO_2(110) surfaces of interest by means of DFT calculations (*31*). In some distance of the point defects, all three surfaces can be considered as being stoichiometric [*s*-TiO_2(110)]. In this case, the diffusion barriers are found to be very low (i.e., Au_1 readily diffuses at RT). Diffusion of Au_1 on *s*-TiO_2(110) is possible not only in the [001] direction but also in the [1$\bar{1}$0] direction (Fig. 3A). Previous DFT calculations likewise indicate facile diffusion of small Au particles on stoichiometric oxide surfaces (*20*, *32*–*34*).

For the *h*-TiO_2(110) surface, we reached identical conclusions because the diffusion barriers are almost unchanged (Fig. 3B). However, the Au monomers can be trapped at point defects on the terraces of the *r*- and *o*-TiO_2(110) surfaces (right side of Fig. 3, C and D, respectively). In these cases, the barriers are high enough to prevent diffusion events at RT. These calculations are fully in line with our STM observations of homogeneously distributed small Au nanoclusters exclusively on the *r*- and *o*-TiO_2(110) surfaces and sintering of Au clusters on the *h*-TiO_2(110) surface after Au exposure at RT (Fig. 1).

In Fig. 4, we compare the energetically most favorable Au structures found in DFT calculations with the high-resolution STM images of most abundant small Au_n clusters. On *r*-TiO_2(110), the smallest Au-related protrusions (Fig. 4D) arise from Au_1 in O_{br} vacancies, because the density of these smallest protrusions increases upon Au exposure at the expense of the density of the faint protrusions arising from O_{br} vacancies (*17*, *28*). The second smallest protrusions found (Fig. 4, E and F) originate from linear Au trimers (Au_3). This assignment relies on the following: (i) Au dimers (Au_2) are calculated to adhere less strongly to the support than Au_3 clusters (Table 1), and (ii) DFT calculations of two Au_3 configurations, either symmetrically (Fig. 4B) or asymmetrically (Fig. 4C) attached to the O_{br} vacancy, precisely reproduce the two most abundant protrusions in this size range revealed in the STM measurements.

On the *o*-TiO_2(110) surface, we observed a different distribution of protrusions of Au_n clusters (Fig. 4, J to L), where some of the smallest Au topographies are depicted. Because the O_{ot} atoms serve as nucleation sites for incoming Au_1 (Fig. 3D), the O_{ot} atoms are probably incorporated into the Au_n clusters. A one-to-one assignment of measured protrusions to certain Au_n-O_{ot} clusters is not trivial, but the distinct height distribution of the Au clusters on the *o*-TiO_2(110) surface allows us to distinguish between Au_n clusters consisting of one, two, or even three Au layers (fig. S2).

The DFT results of a more complete survey for stable Au_n clusters with $1 \leq n \leq 5$ and $n = 7$ on the three TiO_2(110) surfaces of interest are summarized in Table 1. As reference, we also considered *s*-TiO_2(110), although this surface was not studied experimentally. The most stable con-

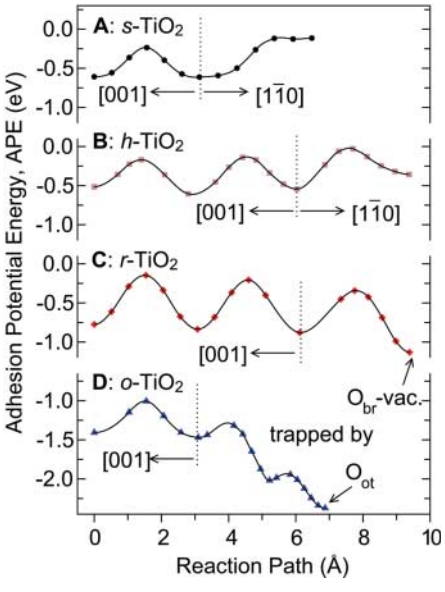

Fig. 3. Potential energy profiles for Au_1 cluster diffusion on *s*- (**A**), *h*- (**B**), *r*- (**C**), and *o*- (**D**) TiO_2(110). The minima at which Au_1 is trapped at the point defects on *r*- and *o*-TiO_2(110) are indicated (arrows; vac. means vacancy). On *s*- and *o*-TiO_2(110), Au_1 diffuses along the O_{br} rows, whereas, on *h*- and *r*-TiO_2(110), Au_1 diffuses along the Ti troughs.

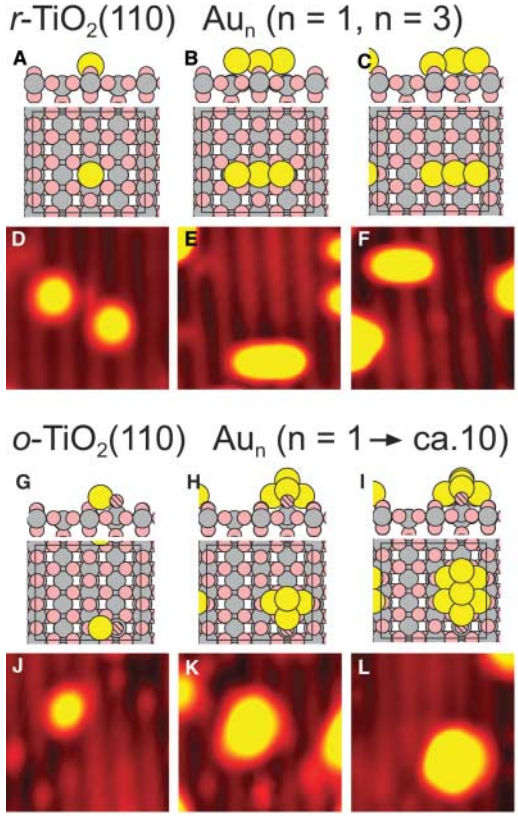

Fig. 4. (Top) Most favorable structures found in DFT calculations for Au_1 trapped in an O_{br} vacancy (**A**), Au_3 symmetrically attached on an O_{br} vacancy (**B**), and nonsymmetrically attached Au_3 (**C**). (**D** to **F**) Zoom-in STM images (40 × 40 Å^2) showing Au_n clusters that are ascribed to the calculated Au_n cluster configurations. Corresponding line profiles to these measurements are shown in fig. S1. (Bottom) Most favorable structures found in DFT calculations for Au_1 (**G**), Au_4 (**H**), and Au_7 (**I**) on *o*-TiO_2(110). (**J** to **L**) Zoom-in STM images (40 × 40 Å^2) of Au_n clusters attached in the vicinity of O_{ot} atoms that are tentatively assigned to the calculated Au_n cluster configurations.

Table 1. DFT-based APEs in eV (per Au_n cluster) of the most stable Au_n clusters with $1 \leq n \leq 5$ and $n = 7$ on *r*-, *h*-, *s*-, and *o*-TiO_2(110) surfaces, respectively. Some of these numbers are plotted in Fig. 5E (see also figs. S3 to S7).

Gold cluster	*r*-TiO_2(110)	*h*-TiO_2(110)	*s*-TiO_2(110)	*o*-TiO_2(110)
Au_1	–1.14	–0.54	–0.61	–2.38
Au_2	–0.71	–0.05	–0.10	–1.94
Au_3	–1.41	–1.26	–1.36	–3.09
Au_4	–0.57	–0.64	–0.97	–4.04
Au_5	–0.31	–1.04	–1.32	–3.57
Au_7	–0.52	–0.87	–1.18	–3.83

figurations on s-TiO_2(110) are two-dimensional (2D) structures that are attached via the O_{br} atoms and thus are aligned in the [001] direction. As reported previously, these structures adhere only weakly (*35*). On the h-TiO_2(110) surface, we found even smaller adhesion potential energies (APEs) for the most stable configurations. In contrast, on the r-TiO_2(110) surface, Au_1 and Au_3 bind relatively strongly in O_{br} vacancies, whereas Au_2, Au_4 (Au tetramers), Au_5 (Au pentamers), and Au_7 (Au septamers) bind very weakly. For the o-TiO_2(110) surface, we found extraordinarily strong bonding of all Au_n clusters considered.

According to the DFT results addressing r- and o-TiO_2(110), the energy for Au_n cluster detachment from the defects on the r-TiO_2(110) surfaces decreases rapidly with cluster size but not on the o-TiO_2(110) surface, where the detachment energy remains high. This means that, for a given Au dispersion, a higher persistence against sintering upon heating is likely to exist on the o-TiO_2(110) surface as compared to the situation on the r-TiO_2(110) surface. Thus, the DFT results presented in Table 1 corroborate the STM findings shown in Fig. 2, C to F.

To gain insight into why the Au_n clusters bind much more strongly on the o-TiO_2(110) surface than on the r-TiO_2(110) surface, we compared electron charge density difference maps for two selected Au_n clusters (Fig. 5, A and C). For the r-TiO_2(110) surface, we chose an Au_3 cluster symmetrically attached in an O_{br} vacancy, because we observed this cluster with the STM (Fig. 4E). Analyzing the bonding qualitatively in three dimensions (Fig. 5A), we found that electron charge accumulates (red isosurfaces) between the Au atoms and the substrate 5f-Ti upon adsorption, indicating the formation of covalent bonds. A more quantitative analysis, where we only considered the charge redistribution perpendicular to the support, shows that the Au atoms primarily experience charge polarization upon adsorption (Fig. 5B).

On the o-TiO_2(110) surface, we studied the extraordinarily stable Au_4 cluster in the vicinity of an O_{ot} atom. In this case, charge redistribution is seen along the Au–O bond axes (Fig. 5C), indicating that the Au–O bonds contribute to the attachment of the Au_4 cluster. The quantitative analysis (Fig. 5D) reveals that electron charge has indeed been transferred to the surface O atoms, whereby the Au_4 cluster has become cationic. This means that the bonding of Au_4 on the o-TiO_2(110) surface is partially ionic.

Contribution of ionic bonding in the case of Au_4 on o-TiO_2(110) is consistent with the calculated atomic Au 5d populations upon adsorption of Au_3 and Au_4 on the r- and o-TiO_2(110) surfaces, respectively. As compared to Au_3 and Au_4 in the gas phase, the total 5d population is reduced by 0.24 and 0.56 e^- for Au_3/r-TiO_2(110) and Au_4/o-TiO_2(110), respectively (*36*). The larger reduction of the 5d populations for Au_4/o-TiO_2(110) can be traced back mainly to the single Au atom that binds directly to the O_{ot} atom, because this Au atom contributes 0.22 of the 0.56 e^-.

The different bond mechanisms of the considered Au_n clusters (Fig. 5, A to D) reflect that the reduced r- and h-TiO_2(110) surfaces are electron rich (formally having two and one excess electrons per O_{br} vacancy and OH_{br} species, respectively), whereas the o-TiO_2(110) surface is electron deficient (formally missing two electrons per O_{ot} atom). As a function of the surface oxidation state, the Au_n-TiO_2(110) adhesion is nonmonotonic for n = 1, 2, and 3 with the lowest adhesion strengths on the h- and s-TiO_2(110) surfaces (Fig. 5E). For these small Au_n clusters, the adhesion strength increases on r-TiO_2(110), because the covalent bonds between Ti and Au form more readily when not all of the Ti atoms are in their fully oxidized state. However, an adhesion mechanism involving cationic Au occurs when the surface is oxidized [o-TiO_2(110)], which leads to a much stronger Au_n-support bonding than that on the r-TiO_2(110) surface.

In light of the presented experimental and computational results, we doubt that O vacancies on oxide surfaces are relevant at all for the stabilization of dispersed Au particles under real reaction conditions with usually high oxygen pressures. Instead, our results suggest that, even under slightly oxidizing conditions as used here, the Au particles are stabilized via Au–O–M bonds (where M represents a metal atom of the supporting oxide). This interpretation is in line with recent reports on cationic Au species for Au supported on magnesia (*11*), ceria (*12*, *15*), and iron oxide (*14*).

In all of the model studies addressing Au supported on titania where the catalytic activity of the systems considered was shown, very high oxygen exposures had been used to prepare or to "activate" the catalysts (*7*, *8*, *18*, *23*). This observation is an additional reason why we question previously proposed structure models, including our own (*17*, *35*), where it was implied that in O vacancies attached Au clusters cause the catalytic activity in "real" catalysts (i.e., at high pressure). We propose that Au particles dispersed on reducible oxides are better catalysts than those supported on nonreducible ones, because reducible oxides are more capable

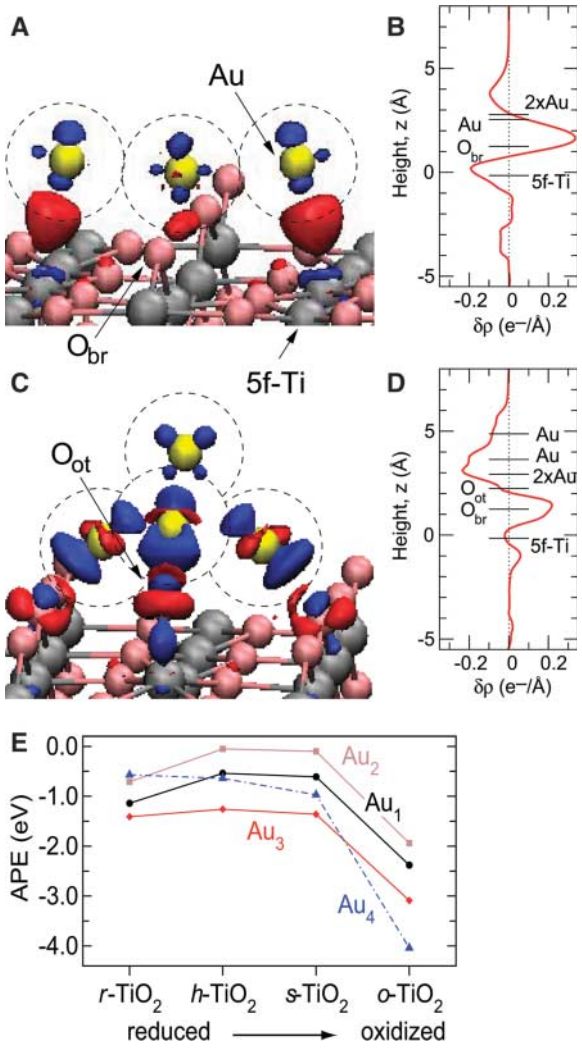

Fig. 5. (**A**) Charge density difference map of an Au_3 cluster attached to an O_{br} vacancy. Yellow spheres and dashed circles mark positions of Au atoms. Blue and red isosurfaces indicate depletion and addition, respectively, of 0.05 e^- per $Å^3$. (**C**) Charge density difference map of Au_4 attached on o-TiO_2(110). Isosurfaces are defined as in (A). (**B** and **D**) Electron charge density difference ($\delta\rho$) for the same systems as in (A) and (C), respectively, but integrated over the x and y dimensions of the super cell. The z positions of O and Au atoms are given with respect to the 5f-Ti atoms (z = 0), whereby the label "2 × Au" is used to indicate the z positions of the two Au atoms that have identical z values in the two Au_n clusters considered. (**E**) Plot of the calculated APEs for the most stable small Au_n clusters (n = 1 to 4) as a function of the "TiO_2(110) oxidation state" (compare with Table 1).

of forming O-rich Au–support interfaces. Note that O-rich surface terminations have been identified not only for titania (*24*, *37*) but also for several other reducible oxides, including vanadium and iron oxide (*38*).

A much stronger Au oxide–support adhesion exists on O-rich Au–support interfaces than on O-poor oxide–support surfaces. For catalytic applications, this result suggests the occurrence of cationic gold at the Au-support interface as a general feature. For the *r*-TiO_2(110) surface, we found that O_{br} vacancies allow for the stabilization of gold monomers and gold trimers, but larger gold clusters cannot be sufficiently stabilized. We emphasize that our approach of studying the oxide support in a range of oxidation states is applicable to numerous other model systems.

References and Notes

1. M. Haruta, N. Yamada, T. Kobayashi, S. Iijima, *J. Catal.* **115**, 301 (1989).
2. G. C. Bond, D. T. Thompson, *Gold Bull.* **33**, 41 (2000).
3. F. Cosandey, T. E. Madey, *Surf. Rev. Lett.* **8**, 73 (2001).
4. R. Meyer, C. Lemire, Sh. K. Shaikhutdinov, H.-J. Freund, *Gold Bull.* **37**, 72 (2004).
5. U. Diebold, *Surf. Sci. Rep.* **48**, 53 (2003).
6. G. R. Bamwenda, S. Tsubota, T. Nakamura, M. Haruta, *Catal. Lett.* **44**, 83 (1997).
7. M. Valden, X. Lai, K. Luo, Q. Guo, D. W. Goodman, *Science* **281**, 1647 (1998).
8. S. Lee, C. Fan, T. Wu, S. L. Anderson, *J. Am. Chem. Soc.* **126**, 5682 (2004).
9. M. M. Schubert *et al.*, *J. Catal.* **197**, 113 (2001).
10. S. H. Overbury *et al.*, *Catal. Lett.* **95**, 99 (2004).
11. J. Guzman, B. C. Gates, *J. Am. Chem. Soc.* **126**, 2672 (2004).
12. Q. Fu, H. Saltsburg, M. Flytzani-Stephanopoulos, *Science* **301**, 935 (2003).
13. L. Fu *et al.*, *J. Phys. Chem. B* **109**, 3704 (2005).
14. G. J. Hutchings *et al.*, *J. Catal.* **242**, 71 (2006).
15. J. Guzman, S. Carrettin, A. Corma, *J. Am. Chem. Soc.* **127**, 3286 (2005).
16. J. G. Wang, B. Hammer, *Phys. Rev. Lett.* **97**, 136107 (2006).
17. E. Wahlström *et al.*, *Phys. Rev. Lett.* **90**, 026101 (2003).
18. M. S. Chen, D. W. Goodman, *Science* **306**, 252 (2004).
19. I. N. Remediakis, N. Lopez, J. K. Nørskov, *Angew. Chem. Int. Ed.* **44**, 1824 (2005).
20. A. S. Wörz, U. Heiz, F. Cinquini, G. Pacchioni, *J. Phys. Chem. B* **109**, 18418 (2005).
21. F. Boccuzzi, A. Chiorino, *J. Phys. Chem. B* **104**, 5414 (2000).
22. B. Schumacher, V. Plzak, M. Kinne, R. J. Behm, *Catal. Lett.* **89**, 109 (2003).
23. T. S. Kim, J. S. Stiehl, C. T. Reeves, R. J. Meyer, C. B. Mullins, *J. Am. Chem. Soc.* **125**, 2018 (2003).
24. S. Wendt *et al.*, *Surf. Sci.* **598**, 226 (2005).
25. Materials and methods are available as supporting material on *Science* Online.
26. O. Bikondoa *et al.*, *Nat. Mater.* **5**, 189 (2006).
27. W. S. Epling, C. H. F. Peden, M. A. Henderson, U. Diebold, *Surf. Sci.* **412-413**, 333 (1998).
28. When we compared the herein-presented comprehensive data set with previous data from our group (*17*), it became apparent that, in (*17*), Au was evaporated onto TiO_2(110) surfaces of various character. For the low-temperature experiments in (*17*), the starting point was a clean *r*-TiO_2(110) surface. For the Au exposures at higher temperatures, however, unintentionally *h*-TiO_2(110) surfaces were used. Taking this into account, there is full agreement between the STM results in (*17*) and the present work. In both data sets, ~80% of the Au clusters were found at the step edges after Au exposure onto *h*-TiO_2(110) at RT.
29. X. Tong *et al.*, *J. Am. Chem. Soc.* **127**, 13516 (2005).
30. C. T. Campbell, S. C. Parker, D. E. Starr, *Science* **298**, 811 (2002).
31. The Au_n APEs on the various TiO_2(110) supports were calculated according to APE = E_{tot} (Au_n + support) − E_{tot} (Au_n) − E_{tot} (support), where E_{tot} (Au_n + support), E_{tot} (Au_n), and E_{tot} (support) are the total energies of the combined systems, the most stable gas phase Au_n 2D clusters, and the TiO_2(110) surface in a certain oxidation state, respectively. Negative APEs indicate stable adhesion of the Au_n clusters. For details, see (*25*).
32. A. Del Vitto, G. Pacchioni, F. Delbecq, P. Sautet, *J. Phys. Chem. B* **109**, 8040 (2005).
33. H. Iddir, S. Öğüt, N. D. Browning, M. M. Disko, *Phys. Rev. B* **72**, 081407(R) (2005).
34. H. Iddir, S. Öğüt, N. D. Browning, M. M. Disko, *Phys. Rev. B* **73**, 039902(E) (2006).
35. L. M. Molina, M. D. Rasmussen, B. Hammer, *J. Chem. Phys.* **120**, 7673 (2004).
36. Changes in the Au 6s and 6p populations also occur and must be in the order of 0.25 e^- accumulation per Au cluster for Au_3/*r*-TiO_2(110) in order to conform with Fig. 4D, where only charge polarization and no net charging is shown. The changes in the Au 6s and 6p populations cannot be quantified because these orbitals overlap substantially with other orbitals originating from neighboring atoms.
37. T. J. Beck *et al.*, *Phys. Rev. Lett.* **93**, 036104 (2004).
38. M. Abu Haija *et al.*, *Surf. Sci.* **600**, 1497 (2006), and references therein.

39. We acknowledge financial support from the Danish Ministry of Science, Technology, and Innovation through iNANO, the Danish Research Councils, and the Danish Center for Scientific Computing. D.M. acknowledges support from the Swiss National Science Foundation. We thank D. W. Goodman for fruitful discussions.

Supporting Online Material

www.sciencemag.org/cgi/content/full/315/5819/1692/DC1
Materials and Methods
Figs. S1 to S7
References

2 October 2006; accepted 9 February 2007
10.1126/science.1135752

An Atomic Seesaw Switch Formed by Tilted Asymmetric Sn-Ge Dimers on a Ge (001) Surface

K. Tomatsu,[1] K. Nakatsuji,[1] T. Iimori,[1] Y. Takagi,[2] H. Kusuhara,[3] A. Ishii,[3] F. Komori[1]

When tin (Sn) atoms are deposited on a clean germanium (Ge) (001) surface at room temperature, buckled dimers originating from the Sn atoms are formed at the Ge-dimer position. We identified the dimer as a heterogeneous Sn-Ge dimer by reversing its buckling orientation with a scanning tunneling microscope (STM) at 80 kelvin. An atomic seesaw switch was formed for one-dimensional electronic conduction in the Ge dimer–row direction by using the STM to reversibly flip the buckling orientation of the Sn-Ge dimer and to set up standing-wave states.

Considerable effort has been devoted to the switching of electronic conduction through the movement of atoms. Atomic switches have been formed between two electrodes (such as a metal tip and a metal surface) by controlling the surface migration of atoms or the formation and annihilation of an atomic bridge (*1*–*5*). A molecular conformation change has been proposed to create another type of nanoscale switch (a molecular switch) (*6*–*11*). However, the direct observation of different conducting pathways with atomic resolution has been difficult to achieve. One difficulty in correlating changes in atomic positions with changes in conductivity is that in most of the systems that have been studied, the conducting pathway is perpendicular to the direction that can be imaged with scanning probe methods, or the switching between conducting and nonconducting configurations is not reversible. We now report the observation of switching between conducting and nonconducting states of one-dimensional (1D) rows of dimers on a semiconducting Ge (001) surface on which a sparse coverage of Sn atoms had been deposited. These adatoms incorporate into the dimer rows to create buckled Sn-Ge dimers that can adopt two different configurations that can be switched reversibly with a scanning tunneling microscope (STM) tip. We find that one of these configurations maintains the conductive free-electron state, whereas the other reflects the conduction electrons and sets up a standing-wave state.

On a clean Ge (001) surface, two atoms form a dimer with multiple bonds of π and σ conjugations. The dimer tilts (buckles) from the surface plane, and the bonding π and antibonding π* states localize on the upper and lower atoms of the dimer, respectively (*12*). The Ge dimers align in the [110] direction, forming a dimer row. The neighboring dimers in the same dimer row are buckled in the opposite configuration, and the π* electron behaves like a 1D free electron along the dimer row (*13*). It was recently shown that the buckling orientation of the Ge dimer can be reversibly controlled by a surface bias voltage of the STM (*14*). This conformation change is induced by inelastic scattering of injected carriers from the STM tip to the surface under the electric field, as a result of the bias voltage.

[1]Institute for Solid State Physics, University of Tokyo, 5-1-5 Kashiwanoha, Kashiwa-shi, Chiba 277-8581, Japan. [2]RIKEN Harima Institute at Spring-8, 1-1-1 Kouto, Mikazuki-cho, Sayo-gun, Hyogo 679-5148, Japan. [3]Department of Applied Mathematics and Physics, Tottori University, 4-101 Minami, Koyama, Tottori 680- 8552, Japan.